Electrochimica Acta 298 (2019) 858–865

Contents lists available at ScienceDirect

Electrochimica Acta

journal homepage: www.elsevier.com/locate/electacta

Applying the deconvolution approach in order to enhance RRDE time resolution: Experimental noise and imposed limitations

Artem V. Sergeev [a, b, *], Tatiana K. Zakharchenko [c, d], Alexander V. Chertovich [b], Daniil M. Itkis [c, d]

[a] Skolkovo Institute of Science and Technology, Moscow, 143026 Russia
[b] Physics Department, Lomonosov Moscow State University, Moscow, 119991 Russia
[c] Materials Science Department, Lomonosov Moscow State University, Moscow, 119991 Russia
[d] Chemistry Department, Lomonosov Moscow State University, Moscow, 119991 Russia

ARTICLE INFO

Article history:
Received 20 August 2018
Received in revised form
10 December 2018
Accepted 24 December 2018
Available online 26 December 2018

Keywords:
RRDE
Deconvolution
Impulse response function
Passivation
Adsorption

ABSTRACT

The ring electrode of an RRDE setup is commonly used to detect redox active species produced at the disk electrode. It is especially useful when some side processes occur at the disk (e.g. passivation film growth) along with a main electrochemical reaction of interest, which produces a soluble redox-active specie. Unfortunately, the detected ring current signal is a delayed and smeared-out representation of the disk faradaic process so that fast changes of its magnitude cannot be studied. The deconvolution approach is a mathematical data processing procedure that enables reconstruction of the disk signal with a hypothetically infinite accuracy. There are, however, practical limitations arising mainly from inevitable presence of noise in the measured ring current used for the reconstruction. In this paper the deconvolution approach is discussed in details and its applicability is investigated basing on a series of experiments with a model system. A procedure to filter out spurious artifacts from the reconstructed disk signal is proposed and tested.

1. Introduction

A rotating ring-disk electrode (RRDE) invented by Frumkin and Nekrasov [1] enables detection of a product of the electrochemical reaction occurring at the disk by facilitating a reverse electrochemical reaction at the ring. It is especially useful when more than one processes occur at the disk. In such a case there are two contributions to the disc current. First is associated with the generation of a main reaction product, which is emitted into the solution. Another contribution comes from the other side processes such as a passivation film growth or production of a specie that cannot be detected at the ring. The disk current fraction associated with the main process can be easily determined by simple dividing the ring current by the RRDE collection efficiency parameter. The result can be then subtracted from the total disk current yielding the side processes contribution.

RRDE is widely used for solving a variety of research problems such as metal and alloy plating [2,3] and stripping [4,5], metal underpotential deposition [6], oxidation of soluble molecules [7,8], electrochemical water splitting [9–11], reduction of oxygen [12–15] and sulfur [16].

Although most commonly the RRDE technique is applied for the steady state problems (as mentioned above), additional useful information can be extracted from chronoamperometric response. For example, the chronoamperometric measurements were carried out to investigate underpotential deposition of metals [17,18]. In this works, however, the characteristic time of the studied electrochemical processes is much longer than the RRDE transit time [19], i.e. the time gap between the start of the product emission from the disk into the solution and the moment, when the product reaches the ring. In the case of quickly changing electrochemical processes at the disk (characteristic time is comparable to RRDE transit time) the current transient at the ring does not represent correctly the time-dependent fraction of the disk current associated with the main electrochemical process of interest thus manifesting limited time resolution of the RRDE measurements.

One of the examples, in which the time resolution is quite critical, is the RRDE investigations of oxygen redox in aprotic media,

* Corresponding author. Center for Electrochemical Energy Storage, Skolkovo Institute of Science and Technology, 3 Nobel Str., Moscow, 143026 Russia.
E-mail address: sergeev@polly.phys.msu.ru (A.V. Sergeev).

https://doi.org/10.1016/j.electacta.2018.12.124
0013-4686/

e.g. in the Li-air battery research. At the Li-air cathode two electrochemical process seem to occur simultaneously: first is oxygen reduction to superoxide species ($O_2 + e^- + Li^+ \rightarrow LiO_2$) [20–23] and, second, LiO_2 reduction to Li_2O_2 ($LiO_2 + e^- + Li^+ \rightarrow Li_2O_2\downarrow$) [24–26]. The first reduction produces a flux of soluble LiO_2 that can be detected by electrooxidation at the ring. Unfortunately, the second reduction partially consumes the product of the first electrochemical reaction and results in growth of a passivating Li_2O_2 film. Upon forming the first molecular layers of the Li_2O_2 film (i.e. upon transition from a bare electrode surface to a Li_2O_2 surface), the ratio between the two electrochemical processes can shift drastically while the ring current may not reflect correctly such a quick change. That is supported by the experimental chronoamperometric transients obtained by Torres et al. [27] Instead of monotonous increase until reaching its maximum value (as one would expect in absence of side processes at the disk), the measured ring current exhibits a prominent peak and in some cases decays to zero in spite the disk current is still significant. The peak can be as narrow as 1.5 s (half-height width), which is comparable with the RRDE transit time.

Another vast area, in which RRDE time resolution might be insufficient, is the metal corrosion studies. During an anodic process, the generated metal ions can react with the media causing a passivating film growth, e.g. a layer of iron oxides and hydroxides passivating the iron surface [28,29]. The very onset of the film growth takes a short time and cannot be detected by measuring the ring current. Using a split RRDE Strehblow et al. [30] showed that during anodization of copper disk Cu^+ and CuO_2^{2-} evolve in solution along with formation of CuO and Cu_2O film on copper surface. It was found that due to the high oxide growth rate at initial step of anodization, narrow (FWHM about 1 s) peak is observed on the ring current response, which corresponds to formation of the soluble Cu^+ species.

When investigating adsorption/desorption of redox-active species at the disk electrode one also might face limited time resolution as the characteristic time of such processes can be as short as 0.1–0.5 s (see e.g. Ref. [31]). For such cases it was suggested to account for the transit time in order to estimate the total amount of an adsorbed specie [32].

The most quantitatively accurate way to reconstruct the time-dependent fraction of the disk current associated with the main process of interest employs the deconvolution approach that originates from the signal processing theory. In the framework of the deconvolution approach an RRDE is considered as a linear system that transforms an input signal (i.e. a molar flux of the electrochemically active product from the disk) into the output signal (i.e. a ring molar flux proportional to the ring current). To solve the inverse problem of reconstructing the input signal the method relies on the impulse response function (IRF) of the system that is essentially a 'rule', by which an input signal is transformed into the output signal. The IRF would depend on the RRDE geometry as well as on the solution properties. The deconvolution approach allows one to reconstruct the main fraction of the disk current (associated with an emission of the redox-active product) as a function of time with hypothetically unlimited time resolution. As a basic idea such an approach for RRDE data analysis was firstly considered in Ref. [33], however, the suggested procedures didn't take the noise filtering issue into account while it turned out to be crucial for practical application and, in fact, limits the real-life time resolution that can be achieved. We believe that the lack of practical considerations might be the reason why the deconvolution technique was not widely appreciated by the community and, to the best of our knowledge, this original approach is still not actively used.

Here, we consider the problems one would face trying to employ the deconvolution approach, and demonstrate the application of this tool using the model experiments. A simple redox couple (ferricyanide/ferrocyanide) was chosen for evaluation of the reconstruction results accuracy. First of all, we proposed a procedure to eliminate spurious artifacts from the reconstructed disk current, which arise from the noise inevitably present in the experimentally measured ring current. The practical time resolution limit was estimated and shown to be dependent on the noise in the experimental data. Finally, we investigate transferability of the measured IRF between solutions with different properties. We also present a work-flow plan for application of the deconvolution approach to a chronoamperometric RRDE measurement.

2. Theory

2.1. Introduction of the concept

The deconvolution approach is based on the use of an impulse response function of an RRDE apparatus. Let us think of an abstract system that transforms an input signal $x(t)$ into the output signal $y(t)$. If the system is linear and time-invariant, such transformation can be represented as a convolution:

$$y(t) = x(t)*h(t) = \int_{-\infty}^{+\infty} h(\tau)x(t-\tau)d\tau, \quad (1)$$

where $h(t)$ is the system's IRF, that is a system's output in response to the input of Dirac delta function $\delta(t)$. According to the convolution theorem the above integration (1) can be carried out in frequency domain by simple multiplication of the Fourier transforms (denoted by 'hat' accent ˆ):

$$\widehat{y}(f) = \widehat{x}(f)\widehat{h}(f) \quad (2)$$

The latter allows us to solve a reverse problem, i.e. to find the input $x(t)$ if the output $y(t)$ and the IRF $h(t)$ are known:

$$x(t) = F^{-1}\left\{\frac{\widehat{y}(f)}{\widehat{h}(f)}\right\} \quad (3a)$$

where F^{-1} denotes an inverse Fourier transform.

More details can be found in the signal processing literature, e.g. in Ref. [34].

This theory is applicable to an RRDE as Faradaic currents, diffusion and convection fluxes are linear in respect to the redox specie concentration. Rotation speed, temperature and other external conditions must be kept constant to maintain time invariance.

2.2. Typical application case

We start with a general description of the electrochemical system illustrated in Fig. 1: let's assume that the specie A reduces at the disk producing a flux $j_d(t)$ of soluble A^- outgoing from the disk into the solution bulk. This process is considered to be *main* process of our interest and accounts for the $I_{d\_main}(t)$ component of the disk current. Oxidation of A at the ring produces the ring current proportional to the flux $j_r(t)$ toward the ring surface.

The *side* reaction produces the specie B that cannot be detected at the ring either because it does not undergo electrochemical oxidation under the selected ring potential or because it stays at the disk surface in the form of a passivating layer. Multiple side processes can proceed as well, and all their contribution to the disk

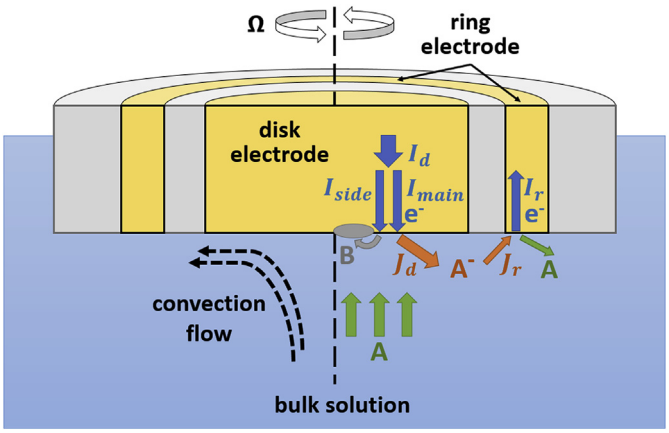

Fig. 1. A schematic representation of the considered electrochemical reactions in an RRDE setup.

current is included in the $I_{d\_side}(t)$.

Disk: main reaction: $A + e^- \rightarrow A^-$; side reaction: $B0 + e^- \rightarrow B$; $I_d(t) = I_{d\_main}(t) + I_{d\_side}(t)$, $I_{d\_main}(t) = j_d(t)F$, where F is the Faraday constant.

Ring: $A^- \rightarrow A + e^-$; $I_r(t) = j_r(t)F$.

When applying the deconvolution approach $I_{d\_main}(t)$ (or $j_d(t)$) should be considered as an input signal $x(t)$, while $I_r(t)$ (or $j_r(t)$) – as an output signal $y(t)$. Thus, the disk main reaction current can be reconstructed as:

$$I_{d\_main}(t) = F^{-1}\left\{\frac{\widehat{I_r}(f)}{\widehat{h}(f)}\right\} \tag{3b}$$

2.3. IRF calculation and correction

Before applying the deconvolution approach the IRF of the investigated system should be calculated. It can be done by solving another reverse problem with the help of the equation similar to eq. (3b):

$$h(t) = \left|F^{-1}\left\{\frac{\widehat{I_r}(f)}{\widehat{I_d}(f)}\right\}\right| \tag{4}$$

Although the IRF must be a real function, due to unavoidable addition of noise to the measured $I_d(t)$ and $I_r(t)$ the result of the inverse Fourier transform most probably will be a complex signal. Therefore, we recommend to use the current absolute value.

The test signal $I_d(t)$ used for the purpose of determining the IRF should be as broad in frequency domain as possible (i.e. the signal and/or it's time derivative should contain short high amplitude pulses). A suitable and easily implemented disk test signal is one generated by potential step technique, as presented in Fig. 2A. (One can try to implement even shorter pulse by swiftly switching the disk potential on and off, but resetting the potential may induce artifacts in both disk and ring signals, so that applicability of such technique would depend on the particular experimental equipment used). The ring current response to the disk potential step signal is provided in Fig. 2B. The typical RRDE's impulse response functions $h(t)$ calculated according to eq. (4) are presented in Fig. 2C.

Unfortunately, the IRF cannot be measured directly for complex systems as it would be affected by side processes at the disk (e.g. passivation film growth), which are to be studied. Therefore, the system should be changed to eliminate the side process. Depending on the situation it can be done by replacing electrode material, by changing electrolyte composition, using another redox-active specie, or by simply measuring IRF at the disk potential values, such that the side process intensity is negligible. For example, in case of Li-O_2 system, one can measure IRF using only background electrolyte without Li^+ cations, thus avoiding Li_2O_2 formation at the disk as a side reaction during oxygen reduction. It should be kept in mind, however, that the oxygen superoxide diffusion coefficient would depend on electrolyte composition due to possible association with cations.

If the solution composition is changed, the measured IRF should be corrected for the difference in kinematic viscosity ν and diffusion coefficient D of the redox specie. Luckily, as shown in Ref. [35], RRDE transients for different values of ω, ν and D match each other when plotted against the dimensionless time $t\omega(D/\nu)^{1/3}$. The IRF is essentially a time derivative of the transient, therefore, upon changing the parameters (ω, ν or D) it should be rescaled along both axis: abscissa (time) and ordinate (amplitude). Thus, if $h_1(t)$ is measured at ω_1 for a solution with ν_1 and D_1 then the IRF at ω_2 for a solution with ν_2 and D_2 can be calculated as:

$$h_2(t) = h_1\left(t\cdot\frac{\omega_2}{\omega_1}\cdot\sqrt[3]{\frac{\nu_1 D_2}{\nu_2 D_1}}\right)\cdot\frac{\omega_2}{\omega_1}\cdot\sqrt[3]{\frac{\nu_1 D_2}{\nu_2 D_1}} \tag{5}$$

A cubic root dependence decreases sensitivity of the rescaling procedure toward the error of ν and D values. The impact of such error on the accuracy of the disk flux reconstruction will be discussed later.

The IRF also can be calculated by means of computer simulation. Original contribution to RRDE numerical simulation was made by Prater and Bard [36]. Since then a lot of efforts were made [37] to develop more sophisticated and precise numerical models, which take, for example, finite cell dimensions into account. Nevertheless, even simple 2D models are able to predict collection efficiency within 1% accuracy. And, indeed, robustness of all models depends on the accuracy of the input parameters such as redox specie diffusion coefficient (just as the IRF rescaling procedure described above).

2.4. Noise filtering

An RRDE essentially acts as a low-pass filter, i.e. high-frequency components of input disk signal $j_d(t)$ are severely suppressed in the output ring signal $j_r(t)$. This property also manifests in exponential decay of IRF's Fourier transform $\widehat{h}(f)$. The higher the frequency, the smaller the output signal amplitude. In experiments noise inevitably contributes to the output signal. Even if overall noise level is quite low, at high frequencies it overcomes the evanescent true signal. When applying the deconvolution approach to reconstruct the disk signal the high-frequency components are restored by significant amplification. Mathematically (see eq. (3a),(3b)) it is done by dividing $\widehat{y}(f)$ by $\widehat{h}(f)$, which approaches zero at high frequencies. In practice the high-frequency noise components are amplified so that they conceal the true signal (even strong low-frequency components) and make the reconstructed disk signal indistinguishable from white noise (see Fig. S6). This effect seems to be the major issue for applying deconvolution approach.

Fortunately, the high-frequency noise can be filtered out. So the question the cut-off frequency f_{cut} becomes crucial. Obviously, the higher the f_{cut} the stronger the noise. However, if the cut-off frequency is low, the reconstructed disk signal will lack the sharp (high frequency) details of the original disk signal. To correctly

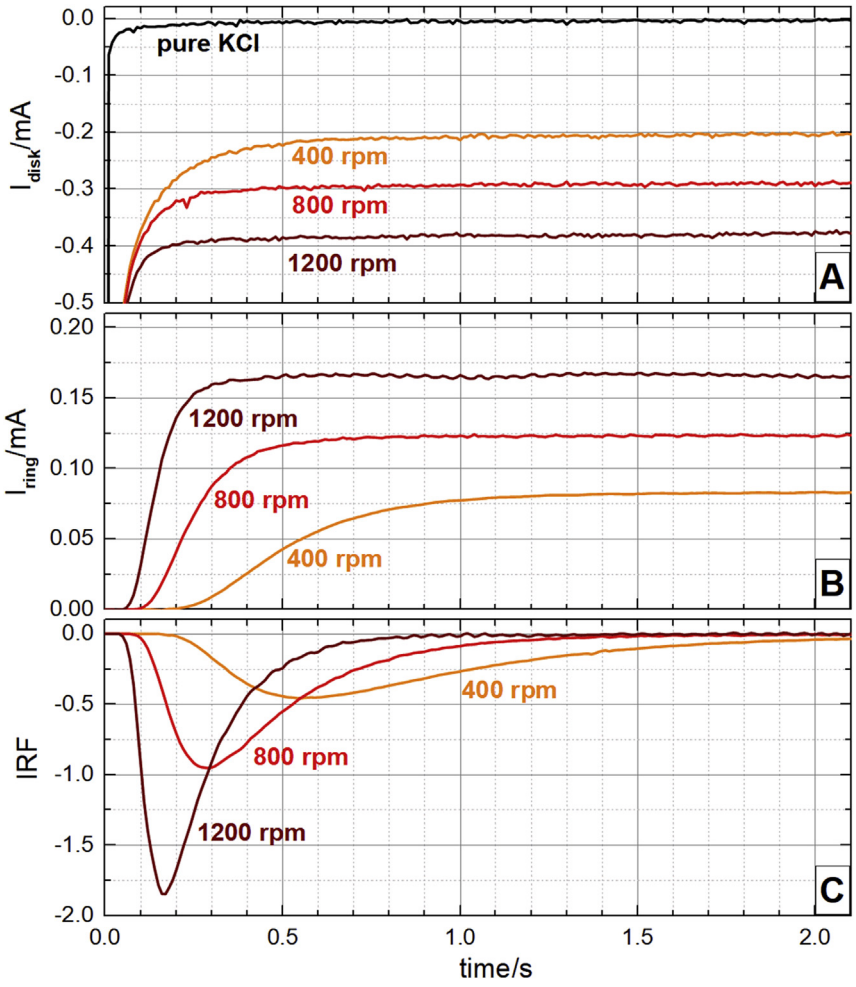

Fig. 2. Currents ((A) – at the disk, (B) – at the ring) measured in response to disk potential step from OCP 0.375 V to −0.5 V vs Ag/AgCl in 5 mM $K_3[Fe(CN)_6]$. The disk current in the pure KCl (without $K_3[Fe(CN)_6]$) solution corresponding to double layer charging process is also presented in (A). (C): Impulse response functions of an RRDE in 5 mM $K_3[Fe(CN)_6]$ calculated according to eq. (4).

choose the f_{cut} we suggest plotting the spectral density of ring signal along with the estimated noise spectral density. That makes it easy to determine at which frequency noise starts to exceed the true signal. Assuming random nature of the noise, its spectral density can be estimated by averaging $I_{r\_n}(t)$ (the measured ring signal that consist of the true ring signal $I_r(t)$ and the noise component $I_n(t)$) over a set of experiments. Upon averaging absolute value of the noise Fourier transform should decrease according to:

$$\left|\left\langle \widehat{I_n}(f)\right\rangle\right| = \left\langle\left|\widehat{I_n}(f)\right|\right\rangle \Big/ \sqrt{M}, \tag{6a}$$

where M is a number of data sets (experiments) to average over. Thus, average noise amplitude for a certain frequency f can be estimated as:

$$\left\langle\left|\widehat{I_n}(f)\right|\right\rangle = \left\langle\left|\widehat{I_{r\_n}}(f) - \widehat{I_{r\_n}}(f)\right|\right\rangle \left(\sqrt{M} \Big/ \left(\sqrt{M} - 1\right)\right) \tag{6b}$$

After that the estimated noise spectral density $P_n(f) = \left|\langle\widehat{I_n}(f)\rangle\right|^2 / T$ can be plotted along with the averaged ring signal spectral density $P_{r\_n}(f) = \left|\langle\widehat{I_{r\_n}}(f)\rangle\right|^2 / T$ to estimate the f_{cut}, at which a desired signal to noise ratio (SNR) is reached. The minimum characteristic time of a process, that can be studied with the help of the deconvolution approach can be estimated as $T_c = 1/f_{cut}$ and therefore, depends on the nosiness of the signal and the number of experimental data sets M to average over. According to our tests even 3 data sets provide a reasonable noise estimation, while there is no need in more than 10 data sets at all.

Finally, before attempting to apply the procedures suggested here we encourage the readers to pay attention to a purely technical but crucial issue regarding implied periodicity of discrete signals that is discussed in the Supplementary materials (section "*Discreteness and periodicity*").

3. Experimental

The experimental measurements were performed using RRDE-3A (ALS Co., Ltd) rotator setup and SP-300 (BioLogic Science Instrument SAS) bipotentiostat. Glassy carbon disk (d = 4 mm) surrounded by a Pt ring (d_1 = 5 mm, d_2 = 7 mm) (ALS Co., Ltd) was used as an electrode. It was polished by 0.6 μm silica and ultrasonicated in water prior to experiment. A three-electrode one-compartment electrochemical cell with Pt wire as counter electrode and Ag/AgCl (sat. KCl) (ALS Co., Ltd) as reference electrode was used. 5 mM $K_3[Fe(CN)_6]$ (pure) solution in 1 M KCl supporting electrolyte was prepared using deionized water (Millipore, resistivity >10

MOhm·cm). KCl (pure, Ruskhim) was preliminary purified by recrystallization. Prior to the measurements the cell was purged by Ar (ultrapure, 99.999%) for 40 min. In the course of measurement, the cell was further purged by inert gas. The double-layer charge was estimated from the measurements in 1 M solution of KCl without ferrycianide. The sampling interval of the measured currents did not exceed $\Delta t = 1$ ms.

4. Results and discussion

To calculate the IRF we carried out a series of experiments ($\omega = 400$, 800, 1200 rpm) under potential step condition at the disk (from OCP, which was 0.375 V, to −0.5 V *vs.* Ag/AgCl) resulting in a sharp disk current peak that decays to the steady state value (Fig. 2A). The data were processed according to eq. (4) yielding the IRFs presented in Fig. 2C. High frequency oscillations are observed in the calculated IRFs. Such oscillations are inherited from the ring current signals shown in Fig. 2B. The oscillation frequencies are equal to the corresponding electrode rotation frequencies (rotation speed values used), therefore we attribute this artifact to the imperfections of the electrode geometry that introduce hydrodynamic perturbations affecting the ring current. The presence of such noise components turned out to be one of the major limitation for the time resolution of RRDE approach. The relations between the three calculated IRFs are in good agreement with eq. (5) for scaling in respect to rotation speed (see Fig. S5).

It is worth noticing, that the IRF calculation requires accounting for the electric doubly layer charging (*dlc*). The *dlc* component can be evaluated by applying the same disk potential conditions in the absence of electroactive specie. The disk current measured in such a way (in our case in KCl solution without $Fe(CN)_6^{3-}$ ions) is compared to the originally observed disk currents ($KCl + Fe(CN)_6^{3-}$) in Fig. 2A. The *dlc* component was subtracted from the total disk current before calculating the IRF. The difference between the *dlc*-corrected IRFs and uncorrected ones turned out be negligible due to insignificance of the *dlc* component. Nevertheless, this condition should be checked and efforts should be taken to mitigate *dlc*.

To investigate the applicability of the deconvolution approach, a series of short rectangular pulses was used as a test disk current. The input disk current and the resulted ring current for a single rotation speed are presented in Fig. 3, while the data for other rotation speeds can be found in the Supplementary information (Fig. S1 and S2). The ring current rescaled to compensate for the collection efficiency ($N_{col} = 0.415$, calculated from steady state current values presented in Fig. 2A and B) is also plotted in Fig. 3. Nevertheless, the amplitude of the scaled ring signal is still almost 2 times smaller than the amplitude of the original disk signal as the duration of the rectangular pulses (and delays in-between them) is close to the RRDE transient time. Thus, at the ring the pulses are smeared and averaged. Besides that, the whole series of pulses (the envelope of it) is distorted, falsely asymmetric and shifted. All that is manifestation of insufficient time resolution of the RRDE (for this particular input signal). In contrast to that the disk current reconstructed by means of the deconvolution procedure is depicted in Fig. 3 demonstrates all the meaningful features of the original disk signal: a symmetric series of sharp-fronted pulses with full amplitude and near-zero current in-between the pulses. It indicates that the deconvolution approach enables significant enhancement of the RRDE apparatus time-resolution. The possibility of even more precise reconstruction is limited by inevitable presence of noise in the ring signal.

In order to achieve the presented result the reconstructed signal $I_{d\_rec}(t)$ was filtered by discarding signal components at frequencies higher than $f_{cut} = 3.3$ Hz ($\widehat{I_{d\_rec}}(f > f_{cut}) := 0$). Additionally, we suggest to smooth $I_{d\_rec}(t)$ by running average filter with the window width $T_{ave} = 1/f_{cut}$, as it helps to get rid of the artifacts arose from cutting of high-frequency components of the true signal. Filtering is crucial, as the time domain representation of the unfiltered reconstructed signal is completely overwhelmed with the noise (see Fig. S6). Though the comparison of its power spectral density (Fig. 4A) to the powers spectral density of the true disk signal shows that the low-frequency components are correctly reconstructed (such comparison is possible, as in case of the chosen simple system there is only one redox process and the double layer charging is negligible). The particular value of f_{cut} was determined by comparison the spectral density of the ring signal averaged over $M = 10$ experiments to the noise spectral density estimated according to eq. (6b) (see Fig. 4B). The suggested way of choosing the cutoff frequency does not refer to the unknown (in general case) main fraction of the disk current and indeed resulted in best coincidence between the reconstructed disc signal and the true one. The noise power spectral density depends on the conditions of the particular measurement, so that refining the experimental protocol can increase the necessary value of the cutoff frequency and enhance the time resolution even further. Although a strong noise intensity peak is observed at the frequency of the electrode rotation (the same is true for $\omega = 800$ and 1200 rpm, see the Supplementary materials). Therefore, in practice the electrode rotation frequency ω will probably limit the f_{cut}.

A conventional way to improve RRDE time resolution is the increasing of the rotation speed, as it linearly decreases transient time (though the characteristic time of the studied process may decrease as well). In the framework of the deconvolution approach higher rotation speed also yields higher necessary cutoff frequency.

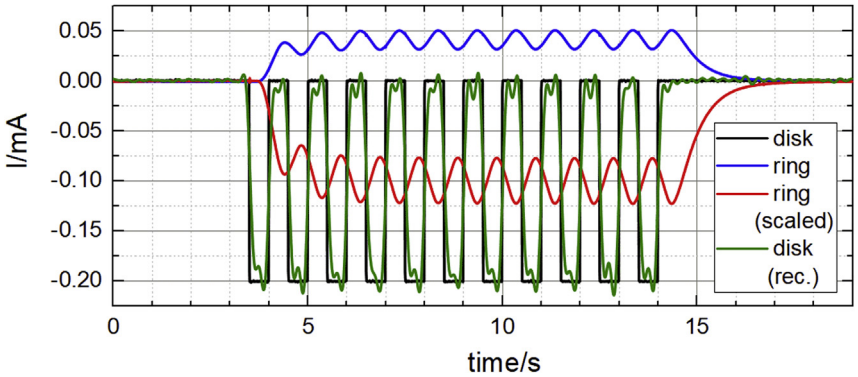

Fig. 3. Experimental results at 400 rpm rotation speed: disk current (black), ring current (blue), scaled ring current ($-I_r/N_{col}$) (red) and reconstructed (and filtered) disk current (green). Ring potential is 0.5 V vs. Ag/AgCl. (For interpretation of the references to colour in this figure legend, the reader is referred to the Web version of this article.)

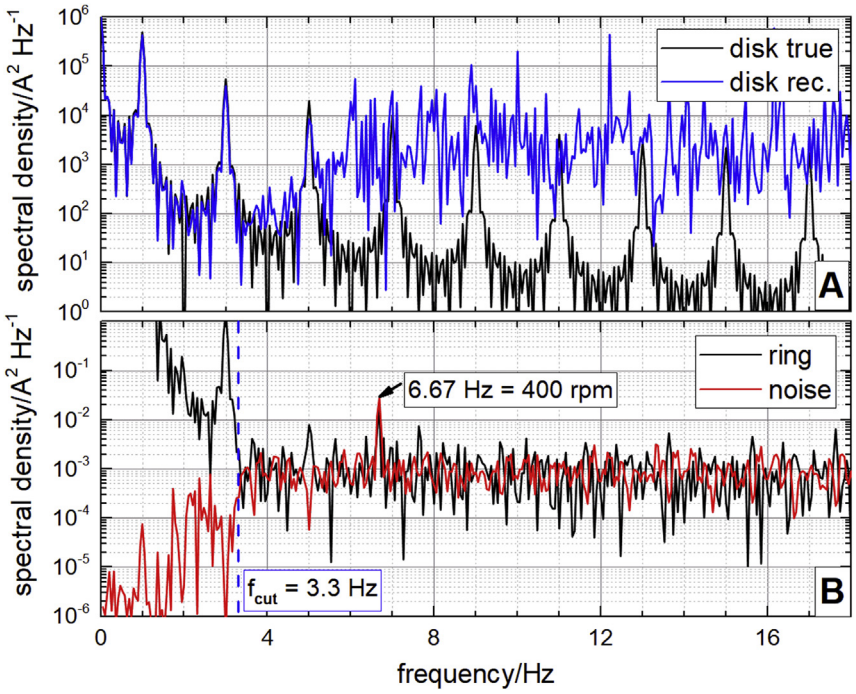

Fig. 4. (A): Power spectral densities of the true disk current (black) and the reconstructed disk current (blue) at 400 rpm rotation speed. (B): Power spectral densities of the averaged ring signal (black) at 400 rpm rotation speed and the estimated noise signal (red). The cutoff and electrode rotation frequencies are marked. (For interpretation of the references to colour in this figure legend, the reader is referred to the Web version of this article.)

The experiments and reconstruction procedure were repeated for $\omega = 400$, 800 and 1200 rpm (see the Supplementary materials), and the estimated cutoff frequencies f_{cut} turned out to be 3.3, 6.4 and 15.1 Hz, respectively. Thus, increasing rotation speed seems to be a viable strategy, though at high ω the signal may become too noisy (in our experiments it occurred at 1800 rpm).

We further investigate the impact of diffusion coefficient D value error on the disk signal reconstruction accuracy. We only consider D assuming kinematic viscosity ν to be known exactly, though all of the following discussion is true for the ratio D/ν. We assign the impulse response function measured at 400 rpm as a reference IRF $h_{ref}(t)$ corresponding to a reference (true) diffusion coefficient value D_{ref}. Then the IRF was recalculated using eq. (4) and a range of diffusion coefficient values. Such distorted IRFs referred to as $h_{cor}(t)$ were used to reconstruct disk signal. The square root of mean square error was used as a measure a reconstruction accuracy ($\sqrt{\text{MSE}} = \sqrt{\int (I_{disk}^{true}(t) - I_{disk}^{reconstruct}(t))^2 dt/T}$). The resulted $\sqrt{\text{MSE}}$ values are plotted in Fig. 5 against diffusion coefficient values used to correct IRF.

To evaluate efficiency of deconvolution approach we compare it to the ring signal shift approach [19,32], in which disk signal can be estimated simply by shifting back the delayed ring signal and scaling it in order to allow for the collection efficiency N_{col}:

$$j_{d\_shift}(t) = j_r\left(t - \tau_{shift}\right)\Big/N_{col} \tag{6}$$

where τ_{shift} is an estimated disk-to-ring delay. A reasonable guess for the τ_{shift} is the transit time [19].

$$\tau_{transit} = 43.1(\nu/D)^{1/3}(\ln r_2/r_1)^{2/3}\Big/\omega\{\text{in rpm}\} \tag{7}$$

where r_1 is disk radius, r_2 is inner ring radius.

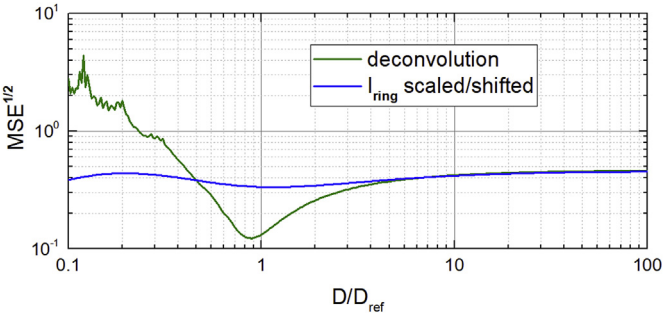

Fig. 5. Mean square error of the reconstructed disk signal as a function of the diffusion coefficient value (related to the true value) used for the reconstruction. Green line – reconstruction by means of the deconvolution approach; blue line – estimation by scaling and shifting the ring signal. (For interpretation of the references to colour in this figure legend, the reader is referred to the Web version of this article.)

According to our calculation the best result in terms of mean square error ($\sqrt{\text{MSE}}$) is achieved for $\tau_{shift} = 1.25\tau_{transit}$, or $\tau_{shift} = 1.20\tau_{peak}$, where τ_{peak} is the time at which IRF reaches its maximum. The shift time τ_{shift} also depends on the diffusion coefficient value. The $\sqrt{\text{MSE}}$ calculated for the ring signal shift approach is presented in Fig. 5 as a function of D value used to estimate τ_{shift}. It should be noted, that the data plotted in Fig. 5 for both approaches are independent of rotation speed ω. The deconvolution approach significantly outperforms the ring signal shift approach if the IRF is accurately corrected for the diffusion coefficient value ($\sqrt{\text{MSE}}$ for the deconvolution approach does not go to zero at $D = D_{ref}$ due to noise). Unfortunately, it loses its efficiency if the estimated D is about 2 times under-/overestimated. Nevertheless, the acceptable error window is wide enough to apply

deconvolution approach in practice.

5. Conclusions

In this paper we discussed practical issues of the deconvolution approach application for reconstructing the disk current associated with the redox specie flux outgoing from the disk as a function of time. The suggested reconstruction procedure is summarized below:

1) Calculating an IRF according to eq. (4). That includes measuring the ring signal in response to a disk potential step. The solution composition and/or the disk potential should be chosen to eliminate side reactions. The ring potential should be set to guarantee a diffusion limited condition.
2) Correcting the IRF according to eq. (5) if the solution composition in the system of interest differs from the solution composition used for measuring the IRF.
3) Performing the measurements of interest with the side reaction taking place. Any current/potential signal (including time dependent function) can be applied at the disk. The ring potential should be set to guarantee diffusion limited condition. The ring current should decay to zero at the end of the measurement (i.e. disk current should be zero before finishing the measurement) in order to avoid discontinuities upon periodical replication. The experiment should be repeated several times (3–10 is recommended).
4) Estimating the noise power spectral density using eq. (6b) ($P_n(f) = |\langle \widehat{I_n}(f) \rangle| /T$) and plotting it along with the power spectral density of the averaged ring signal ($P_r(f) = |\langle \widehat{I_r}(f) \rangle|^2 /T$) in order to find the cut-off frequency f_{cut} at which $P_n(f)$ is still significantly weaker.
5) Reconstructing disc current component $I_{d\_main}(t)$ associated with generation of the reduced (oxidized) dissolved form of the redox-active specie according to eq. (3b).
6) Filtering out high frequency components ($f > f_{cut}$) of the reconstructed disc current. That can be done by truncating Fourier transform of the signal ($\widehat{I_{d\_main}}(f > f_{cut}) := 0$) and additionally applying a running average filter with the window width $T_{ave} = 1/f_{cut}$.
7) The contribution of the side processes into the overall current can be then found by extracting the reconstructed $I_{d\_main}(t)$ from the total disk current: $I_{d\_side}(t) = I_d(t) - I_{d\_main}(t)$.

It was shown that the error of the diffusion coefficient D and viscosity ν values affects the validity of the IRF corrected for the solution composition change or calculated by means of a computer simulation. According to the calculations, the deconvolution approach retains its efficiency if the under-/overestimation of the D/ν ratio does not exceed 2 folds.

Noise influence on the reconstruction result was also analyzed. Filtering out high frequency components was suggested to get rid of spurious artifacts that arise from the noise present in the ring signal. The maximum cutoff frequency, which determines the time resolution of the reconstruction procedure, was shown to depend on the noise spectral density. Finally, a technique was proposed to estimate the noise spectral density through averaging over several experimental data sets. According to the calculations based on the white Gaussian noise model even 2 experiments is enough to roughly estimate the cutoff frequency.

The data and analysis reported in the paper indicate that the deconvolution approach is viable way to significantly enhance RRDE experiment time resolution and has reasonable demands in terms of D/ν ratio error and noise level.

Acknowledgements

The work was financially supported by Centre or Electrochemical Energy of Skolkovo Institute of Science and Technology. The work of T.K. Zakharchenko was supported by the Russian Foundation of Basic Research according to the research project № 18-33-01147.

Appendix A. Supplementary data

Supplementary data to this article can be found online at https://doi.org/10.1016/j.electacta.2018.12.124.

References

[1] A.N. Frumkin, L.N. Nekrasov, On ring disk electrode, Dokl. Akad. Nauk SSSR 126 (1959).
[2] J. Horkans, Determination of partial currents for CuNi and CuCo electrodeposition using rotating ring-disk electrodes, J. Electrochem. Soc. 138 (1991) 411, https://doi.org/10.1149/1.2085600.
[3] Q. Zhu, C.L. Hussey, Galvanostatic pulse plating of bulk Cu-Al alloys on nickel electrodes from room-temperature chloroaluminate molten salts containing benzene, J. Electrochem. Soc. 149 (2002) C268, https://doi.org/10.1149/1.1467941.
[4] H.W. Pickering, C. Wagner, Electrolytic dissolution of binary alloys containing a noble metal, J. Electrochem. Soc. 114 (1967) 698, https://doi.org/10.1149/1.2426709.
[5] S.H. Cadle, S. Bruckenstein, Ring-disk electrode study of the anodic behavior of gold in 0.2M Sulfuric acid, Anal. Chem. 46 (1974) 16–20, https://doi.org/10.1021/ac60337a013.
[6] L.N. Nekrasov, N.P. Berezina, Use of a disc electrode with a ring in studying the electrolytic reduction of copper, Dokl. Akad. Nauk SSSR 142 (1962) 855–858, https://doi.org/10.18287/0134-2452-2015-39-4-453-458.
[7] K. Endo, Y. Katayama, T. Miura, A rotating disk electrode study on the ammonia oxidation, Electrochim. Acta 50 (2005) 2181–2185, https://doi.org/10.1016/j.electacta.2004.09.024.
[8] J. Zhang, C.W. Oloman, Electro-oxidation of carbonate in aqueous solution on a platinum rotating ring disk electrode, J. Appl. Electrochem. 35 (2005) 945–953, https://doi.org/10.1007/s10800-005-7078-2.
[9] J.J. Concepcion, R.A. Binstead, L. Alibabaei, T.J. Meyer, Application of the rotating ring-disc-electrode technique to water oxidation by surface-bound molecular catalysts, Inorg. Chem. 52 (2013) 10744–10746, https://doi.org/10.1021/ic402240t.
[10] T. Poux, A. Bonnefont, G. Kéranguéven, G.A. Tsirlina, E.R. Savinova, Electrocatalytic oxygen reduction reaction on perovskite oxides: series versus direct pathway, ChemPhysChem 15 (2014) 2108–2120, https://doi.org/10.1002/cphc.201402022.
[11] J.T. Mefford, X. Rong, A.M. Abakumov, W.G. Hardin, S. Dai, A.M. Kolpak, K.P. Johnston, K.J. Stevenson, Water electrolysis on $La_{1-x}Sr_xCoO_{3-\delta}$ perovskite electrocatalysts, Nat. Commun. 7 (2016) 11053, https://doi.org/10.1038/ncomms11053.
[12] J.P. Coliman, P. Denisevich, Y. Konai, M. Marrocco, C. Koval, F.C. Anson, Electrode catalysis of the four-electron reduction of oxygen to water by dicobalt face-to-face porphyrins, J. Am. Chem. Soc. 102 (1980) 6027–6036, https://doi.org/10.1021/ja00539a009.
[13] N. Markovic, Kinetics of oxygen reduction on Pt(hkl) electrodes: implications for the crystallite size effect with supported Pt electrocatalysts, J. Electrochem. Soc. 144 (1997) 1591, https://doi.org/10.1149/1.1837646.
[14] U.A. Paulus, T.J. Schmidt, H.A. Gasteiger, R.J. Behm, Oxygen reduction on a high-surface area Pt/Vulcan carbon catalyst: a thin-film rotating ring-disk electrode study, J. Electroanal. Chem. 495 (2001) 134–145, https://doi.org/10.1016/S0022-0728(00)00407-1.
[15] H.M.A. Amin, C. Molls, P.P. Bawol, H. Baltruschat, The impact of solvent properties on the performance of oxygen reduction and evolution in mixed tetraglyme-dimethyl sulfoxide electrolytes for Li-O_2 batteries: mechanism and stability, Electrochim. Acta 245 (2017) 967–980, https://doi.org/10.1016/j.electacta.2017.06.012.
[16] Y.C. Lu, Q. He, H.A. Gasteiger, Probing the lithium-sulfur redox reactions: a rotating-ring disk electrode study, J. Phys. Chem. C 118 (2014) 5733–5741, https://doi.org/10.1021/jp500382s.
[17] G.M. Brisard, E. Zenati, H.A. Gasteiger, N.M. Markovie, P.N. Ross, Underpotential deposition of lead on copper (l11): a study using a single-crystal rotating ring disk electrode and ex situ low-energy electron diffraction and

auger electron spectroscopy, Langmuir 11 (1995) 2221–2230, https://doi.org/10.1021/la00006a060.
[18] S. Bruckenstein, B. Miller, Unraveling reactions with rotating electrodes, Acc. Chem. Res. 10 (1977) 54–61, https://doi.org/10.1021/ar50110a004.
[19] S. Bruckenstein, G.A. Feldman, Radial transport times at rotating ring-disk electrodes. Limitations on the detection of electrode intermediates undergoing homogeneous chemical reacti, J. Electroanal. Chem. 9 (1965) 395–399, https://doi.org/10.1016/0022-0728(65)85037-9.
[20] C.O. Laoire, S. Mukerjee, K.M. Abraham, E.J. Plichta, M.A. Hendrickson, Influence of nonaqueous solvents on the electrochemistry of oxygen in the rechargeable Lithium–Air battery, J. Phys. Chem. C 114 (2010) 9178–9186, https://doi.org/10.1021/jp102019y.
[21] M.J. Trahan, S. Mukerjee, E.J. Plichta, M.A. Hendrickson, K.M. Abraham, Studies of Li-air cells utilizing dimethyl sulfoxide-based electrolyte, J. Electrochem. Soc. 160 (2013) A259–A267, https://doi.org/10.1149/2.048302jes.
[22] D.T. Sawyer, M.J. Gibian, The chemistry of superoxide ion, Tetrahedron 35 (1979) 1471–1481, https://doi.org/10.1016/0040-4020(79)80032-0.
[23] A.I. Belova, D.G. Kwabi, L.V. Yashina, Y. Shao-Horn, D.M. Itkis, On the mechanism of oxygen reduction in aprotic Li-air batteries: the role of carbon electrode surface structure, J. Phys. Chem. C (2017), https://doi.org/10.1021/acs.jpcc.6b12221 acs.jpcc.6b12221.
[24] B.D. McCloskey, R. Scheffler, A. Speidel, G. Girishkumar, A.C. Luntz, On the mechanism of nonaqueous Li-O_2 electrochemistry on C and its kinetic overpotentials: some implications for Li-air batteries, J. Phys. Chem. C 116 (2012) 23897–23905, https://doi.org/10.1021/jp306680f.
[25] V. Viswanathan, K.S. Thygesen, J.S. Hummelshøj, J.K. Nørskov, G. Girishkumar, B.D. McCloskey, A.C. Luntz, Electrical conductivity in Li_2O_2 and its role in determining capacity limitations in non-aqueous Li-O2 batteries, J. Chem. Phys. 135 (2011) 214704, https://doi.org/10.1063/1.3663385.
[26] L. Johnson, C. Li, Z. Liu, Y. Chen, S.A. Freunberger, P.C. Ashok, B.B. Praveen, K. Dholakia, J.-M. Tarascon, P.G. Bruce, The role of LiO_2 solubility in O_2 reduction in aprotic solvents and its consequences for Li-O_2 batteries, Nat. Chem. 6 (2014) 1091–1099, https://doi.org/10.1038/nchem.2101.
[27] W. Torres, N. Mozhzhukhina, A.Y. Tesio, E.J. Calvo, A rotating ring disk electrode study of the oxygen reduction reaction in lithium containing dimethyl sulfoxide electrolyte: role of superoxide, J. Electrochem. Soc. 161 (2014) A2204–A2209, https://doi.org/10.1149/2.0801414jes.
[28] P.C. Andricacos, J. Tabib, L.T. Romankiw, Stripping voltammetry of nickel-iron films electrodeposited on platinum using a rotating-ring-disk electrode, J. Electrochem. Soc. 135 (1988) 1172–1174, https://doi.org/10.1149/1.2095913.
[29] T. Tsuru, E. Fujii, S. Haruyama, Passivation of iron and its cathodic reduction studied with a rotating ring-disk electrode, Corros. Sci. 31 (1990) 655–660, https://doi.org/10.1016/0010-938X(90)90176-6.
[30] H.-H. Strehblow, H.-D. Speckmann, Corrosion and layer formation of passive copper in alkaline solutions, Mater. Corros. Und Korrosion. 35 (1984) 512–519, https://doi.org/10.1002/maco.19840351104.
[31] B.D. Bath, D.J. Michael, B.J. Trafton, J.D. Joseph, P.L. Runnels, R.M. Wightman, Subsecond adsorption and desorption of dopamine at carbon-fiber microelectrodes, Anal. Chem. 72 (2000) 5994–6002, https://doi.org/10.1021/ac000849y.
[32] S. Bruckenstein, D.T. Napp, Theory of adsorption processes at ring-disk electrodes. Application to the adsorption of copper(I) in 0.5 M hydrochloric acid on platinum, J. Am. Chem. Soc. 90 (1968) 6303–6309, https://doi.org/10.1021/ja01025a009.
[33] U. Stöckgen, K.E. Heusler, Mathematical method to eliminate the transfer time from disc to ring at a rotating ring-disc electrode, Electrochim. Acta 44 (1999) 2765–2770, https://doi.org/10.1016/S0013-4686(98)00398-3.
[34] J.C. Santamarina, D. Fratta, Discrete Signals and Inverse Problems an Introduction for Engineers and Scientists, John Wiley & Sons, 2005.
[35] A.J. Bard, L.R. Faulkner, ELECTROCHEMICAL METHODS Fundamentals and Applications, second ed., John Wiley & Sons, New York, 2001.
[36] K.B. Prater, A.J. Bard, Rotating ring-disk electrodes I. Fundamentals of the digital simulation approach. Disk and ring transients and collection efficiencies, J. Electrochem. Soc. 117 (1970) 207, https://doi.org/10.1149/1.2407466.
[37] C. a. Real-Ramirez, J.I. Gonzalez-Trejo, Hydrodynamic analysis of electrochemical cells, in: J. Zhu (Ed.), Computational simulations and applications, In Tech, 2011, pp. 409–426.